Precise tuning of the Curie temperature of (Ga,Mn)As-based magnetic semiconductors by hole compensation: Support for valence-band ferromagnetism

Shengqiang Zhou,[1,*] Lin Li,[1,2] Ye Yuan,[1] A. W. Rushforth,[3] Lin Chen,[4] Yutian Wang,[1] R. Böttger,[1] R. Heller,[1]
Jianhua Zhao,[4] K. W. Edmonds,[3] R. P. Campion,[3] B. L. Gallagher,[3] C. Timm,[5] and M. Helm[1,6]

[1]*Helmholtz-Zentrum Dresden-Rossendorf, Institute of Ion Beam Physics and Materials Research,*
Bautzner Landstrasse 400 01328 Dresden, Germany
[2]*Department of Physics and Electronics, School of Science, Beijing University of Chemical Technology, Beijing 100029, China*
[3]*School of Physics and Astronomy, University of Nottingham, Nottingham NG7 2RD, United Kingdom*
[4]*Institute of Semiconductors, Chinese Academy of Science, Beijing 100080, China*
[5]*Institute of Theoretical Physics, Technische Universität Dresden, 01062 Dresden, Germany*
[6]*Institute of Applied Physics, Technische Universität Dresden, 01062 Dresden, Germany*

For the prototype diluted ferromagnetic semiconductor (Ga,Mn)As, there is a fundamental concern about the electronic states near the Fermi level, i.e., whether the Fermi level resides in a well-separated impurity band derived from Mn doping (impurity-band model) or in the valence band that is already merged with the Mn-derived impurity band (valence-band model). We investigate this question by carefully shifting the Fermi level by means of carrier compensation. We use helium-ion implantation, a standard industry technology, to precisely compensate the hole doping of GaAs-based diluted ferromagnetic semiconductors while keeping the Mn concentration constant. We monitor the change of Curie temperature (T_C) and conductivity. For a broad range of samples including (Ga,Mn)As and (Ga,Mn)(As,P) with various Mn and P concentrations, we observe a smooth decrease of T_C with carrier compensation over a wide temperature range while the conduction is changed from metallic to insulating. The existence of T_C below 10 K is also confirmed in heavily compensated samples. Our experimental results are naturally explained within the valence-band picture.

I. INTRODUCTION

As one of three routes to spintronics [1], diluted ferromagnetic semiconductors (DFS) have been under extensive investigation for two decades [2–5]. Mn-doped GaAs [and its alloys such as Ga(As,P) and Ga(As,Sb)] is regarded as a prototype. Spintronic devices [6–9], hybrid structures [10,11], and other spintronic phenomena [12–14] have been successfully demonstrated. One of the bottlenecks limiting its application is the low Curie temperature T_C, which still does not reach room temperature [15].

Different theoretical models suggest distinct strategies for increasing T_C. In its extreme limit, the impurity-band picture assumes the existence of a separate impurity band formed by Mn-derived dangling-bond hybrid (DBH) states [4,16,17]. In the presence of compensation, the Fermi energy falls into this impurity band. This picture is expected to be correct for weakly doped samples. On the other hand, the extreme valence-band picture proposes that the would-be impurity band is so strongly broadened that it merges with the valence band and does not leave a distinct maximum in the density of states (DOS). The only effect of Mn doping, besides moving the Fermi energy into the merged band, is to create a tail of localized states at the band edge [2,4]. If compensation is not too strong, the states at the Fermi energy are extended and have valence-band character with some admixture of DBHs. There is a continuum of cases connecting these two extremes and some of the controversy [18–28] in the field seems to result from overinterpreting the two pictures. In this work, we use the term "impurity-band picture" to refer to a situation where the impurity band may have merged with the valence band but is still visible by a clear maximum in the DOS. This means that in uncompensated systems, the Fermi energy falls into a minimum of the DOS, where the electronic states show an enhanced tendency towards localization. The low DOS and the localization generically lead to reduced conductivity and magnetic coupling. Hence, within the impurity-band model, T_C is expected to decrease as compensation goes to zero, whereas partial compensation of holes promotes ferromagnetic order and T_C reaches its maximum when the impurity band is roughly half-filled [27,29,30]. Within the valence-band picture, one instead expects the DOS and T_C to increase monotonically with hole concentration. In the extreme limit, Dietl *et al.* [31] and Jungwirth *et al.* [20] indeed predict, within mean-field theory, that T_C increases monotonically with substitutional Mn concentration and with hole concentration.

Even after more than a decade, the question of where the holes are residing is still being debated [18–20,23–28]. One reason for this is that some experimental probes might be more susceptible to DBH-derived properties (for example, local probes at Mn sites) while others see more of the valence-band physics (e.g., transport). Another reason is that the preparation of heavily Mn-doped GaAs is a very delicate procedure, which may result in large variations of sample composition and quality [32,33]. Furthermore, Mn in GaAs acts as an acceptor, resulting in the difficulty to independently control the local-moment and hole concentrations. On the other hand, interstitial Mn ions (Mn_I) are double donors, which, intentionally or unintentionally, compensate the hole doping. Independent precise control of both moment density and hole concentration is required to resolve the "band battle" [28].

*s.zhou@hzdr.de

Four different approaches have been applied to adjust the hole concentration while keeping the Mn concentration constant. Myers *et al.* [34] utilized the As-antisite effect to compensate holes in the low-doping regime of 1%–2% Mn. During growth, they intentionally did not rotate the substrate to obtain a variation of the As to Ga flux ratio, and thereby of the hole concentration, across a single wafer. The second approach is to compensate holes in (Ga,Mn)As by exposing the samples to a hydrogen plasma [35], followed by postannealing [36–38]. In this way, the magnetic and electronic properties of (Ga,Mn)As can be changed qualitatively, though without fine control. On the other hand, the third approach, electrical gating of a (Ga,Mn)As metal-insulator-semiconductor structure, is expected to allow for a fine control over the hole concentration [39], but the required large gate voltage limits this method to samples with relatively low T_C [25]. Finally, it is possible to tune the hole concentration in (Ga,Mn)As by ion irradiation [40–42], which is a standard industry method and allows for a fine tunability and reproducibility. This method is widely used for conventional III-V semiconductors to render a conducting layer highly resistive through the creation of carrier-trapping centers [43,44]. It has been demonstrated to be applicable to (Ga,Mn)As [40–42] and (Ga,Mn)P [45].

In this contribution, we aim to shed light on the debate over the impurity versus valence-band picture for (Ga,Mn)As-based DFS with high Mn concentration. Our approach is to examine the magnetic and transport properties while shifting the Fermi level to higher energies by compensating the free carriers. We demonstrate the possibility of fine-tuning the magnetism of highly conducting (Ga,Mn)As films by ion irradiation. With increasing the displacement per atom (DPA), the (Ga,Mn)As films become gradually more resistive. For a broad range of (Ga,Mn)As and also (Ga,Mn)(As,P) samples, we find universally that T_C *distinctly and monotonically* decreases with increasing DPA, which we interpret in terms of a decreasing free-hole concentration. Our samples are clearly distinct from those studied in Ref. [41], where the magnetization curves become more concave and non-Brillouin-function-like with increasing DPA, while T_C changes relatively little. Even in the strongly insulating regime, we observe values of T_C in the range 5–10 K, unlike in Ref. [46], where T_C suddenly drops to 0 K from around 10–20 K. Taken together with the other observables, e.g., the coercive field and the shape of the magnetization curves, our observations are naturally explained in terms of the valence-band picture but not of the impurity-band picture. This provides support for the former for ferromagnetic (Ga,Mn)As with high Mn concentrations.

II. EXPERIMENT

A. Sample preparation

(Ga,Mn)As films were prepared at the University of Nottingham (UoN), and the Institute of Semiconductors (IOS), Chinese Academy of Sciences. All samples were grown by low-temperature molecular beam epitaxy (MBE) on semi-insulating GaAs(001). The details of the growth of the specific samples is described in the following.

Samples Mn6ann and Mn6ag were grown on low-temperature GaAs buffer layers with a nominal Mn concen-

TABLE I. Sample definitions and related parameters. The ending in sample ID: "ann" means that the sample was annealed at low temperatures for long time, while "ag" means that the samples was as grown.

Sample ID	Stoichiometry	Thickness	Nominal Mn concentration	Initial T_C
Mn6ann	(Ga,Mn)As	25 nm	0.06	129 K
Mn6ag	(Ga,Mn)As	25 nm	0.06	60 K
Mn10ann	(Ga,Mn)As	20 nm	0.10	150 K
Mn6P6ann	(Ga,Mn)As$_{0.94}$P$_{0.06}$	25 nm	0.06	125 K
Mn6P9ann	(Ga,Mn)As$_{0.91}$P$_{0.09}$	7 nm	0.06	80 K

tration of $x = 0.06$ and with a thickness of 25 nm using a Veeco Mod Gen III MBE system at UoN [47]. The Mn concentration was determined from the Mn/Ga flux ratio. The material quality was found to strongly depend on the growth temperature and on the As/Ga flux ratio. The growth temperature of 230 °C is chosen to be the highest possible while maintaining 2D growth, as monitored by reflection high-energy electron diffraction. The films were grown under relatively low As flux to minimize the concentration of As antisites (As$_{Ga}$). The use of As$_2$ as a source instead of As$_4$ also results in lower As$_{Ga}$ concentrations [48]. Sample Mn6ann was annealed in air at 190 °C for 48 hours to remove compensating Mn$_I$. Sample Mn6ag was kept in the as-grown state.

The heavily Mn-doped (Ga,Mn)As film, sample Mn10ann, was grown at 200 °C with a nominal Mn concentration of $x = 0.10$ and a thickness of 20 nm at IOS [49]. During growth, the As/Ga beam equivalent pressure ratio was set to 8. After growth, the sample was annealed at 200 °C for 2 hours in air.

P-alloyed (Ga,Mn)(As,P) samples were grown at UoN. A 50 nm low-temperature GaAs$_{1-y}$P$_y$ buffer layer was grown right before a 25 nm Ga$_{0.94}$Mn$_{0.06}$As$_{1-y}$P$_y$ layer, with nominal concentrations $y = 0.06$ and 0.09 for samples Mn6P6ann and Mn6P9ann, respectively. The buffer and Mn-containing layers were all grown at a low temperature of 230 °C. Both were annealed in air at 190 °C for 48 hours. The sample definitions and the most important parameters are listed in Table I.

B. Ion irradiation

All (Ga,Mn)As wafers were cut into pieces of dimensions of about 5×5 mm^2 for ion irradiation. The He-ion energy was chosen as 4 keV (a few as 650 keV). The details of the irradiation conditions are given in Table II in Appendix A. During ion irradiation, the samples were tilted by 7° to avoid channeling. The samples were pasted onto Si wafers, which were kept at around room temperature without cooling or heating. The resulting defects were found to be distributed roughly uniformly through the whole (Ga,Mn)As layer by simulation using the SRIM (Stopping and Range of Ions in Matter) code [50]. In the following, we refer to the displacement per atom (DPA), which is the number of times that an atom in the target is displaced during irradiation. The DPA is a function of projectile type (ion species, neutron, or light energetic particles), energy, fluence, as well as material properties. In the literature, the calculated DPA is often used as a measure of the irradiation effect in materials. As an example,

for GaAs, 14 He ions of 4 keV will produce a similar DPA as one Ne ion of 20 keV at the same depth. The DPA is a better representation of the effect of irradiation on materials properties than ion fluence (dosage). It allows for a comparison between our results and data reported in the literature, in which often different ion species and energies are used.

By Rutherford backscattering spectroscopy in channeling geometry, which is sensitive to point defects such as Mn interstitials [51–53], we do not observe measurable increase of Mn interstitials even for the largest DPA applied in our work (see Appendix B). In the work of Winkler *et al.* [45], the structural integrity of (Ga,Mn)P after Ar-ion irradiation was confirmed by several techniques. Using ion channeling, the sheet concentration of Mn_{Ga} in their samples was found to remain constant. High-resolution transmission electron microscopy and atomic force microscopy similarly showed no qualitative changes with ion irradiation. Therefore, we can conclude that the effect of He-ion irradiation is mainly to introduce deep traps and thereby compensate the holes. The reduction of hole concentration upon ion irradiation linearly depends on the ion fluence, i.e., the DPA [40,45].

C. Measurements

Magnetic properties were measured with a superconducting quantum interference device (Quantum Design, SQUID-MPMS or SQUID-VSM) magnetometer. To determine T_C, we have measured the temperature-dependent magnetization at a small field of 10 or 20 Oe after cooling down in field. Magnetotransport properties were measured with a magnetic field applied perpendicularly to the film plane in van der Pauw geometry using a commercial Lakeshore Hall System. Fields up to 80 kOe were applied over a wide temperature range from 2.5 to 300 K.

III. RESULTS AND DISCUSSION

Figure 1 shows representatively the temperature-dependent magnetization and the magnetization versus field at 5 K for three samples listed in Table I before and after irradiation at various ion fluences. All measurements were carried out with the field along the magnetic easy axis, which is GaAs[1$\bar{1}$0], except for sample Mn6P9ann, where it is GaAs[001]
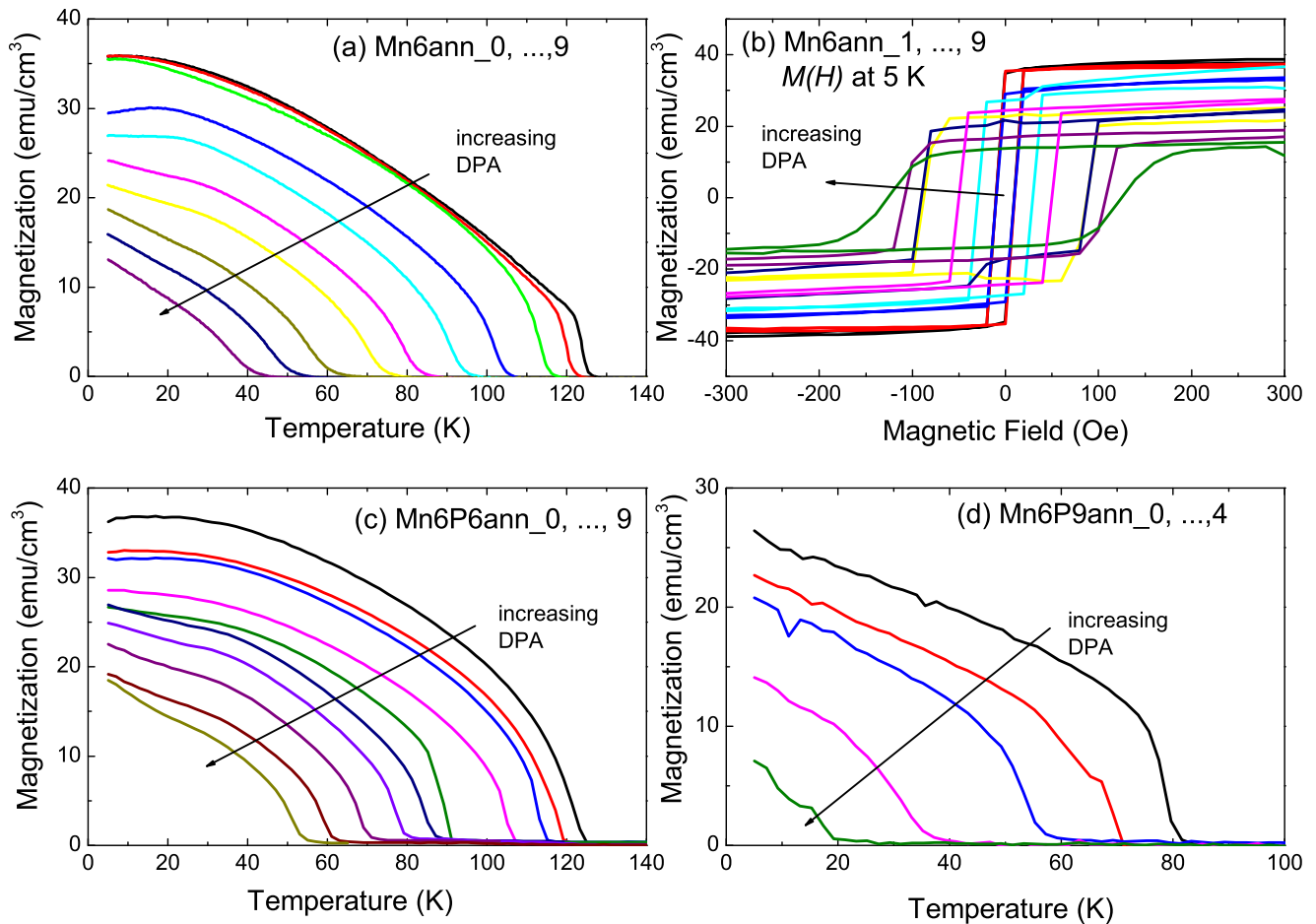

FIG. 1. Magnetic properties after introducing hole compensation by ion irradiation. The ion fluence was increased in linear steps. The hole concentration is expected to decrease linearly depending on DPA [40,45]. (a), (c), and (d) show the temperature dependent magnetization for different samples, while (b) shows the magnetic hysteresis for sample Mn6ann for various ion fluences. The temperature-dependent magnetization is measured at a small field of 20 Oe after cooling in field. One observes an increase in the coercive field H_C when T_C and the remanent magnetization decrease. The arrows indicate the increase of DPA from 0 to 2.88×10^{-3}. The corresponding DPA values are shown in Fig. 2. In each panel, the black line is the result for the nonirradiated sample.
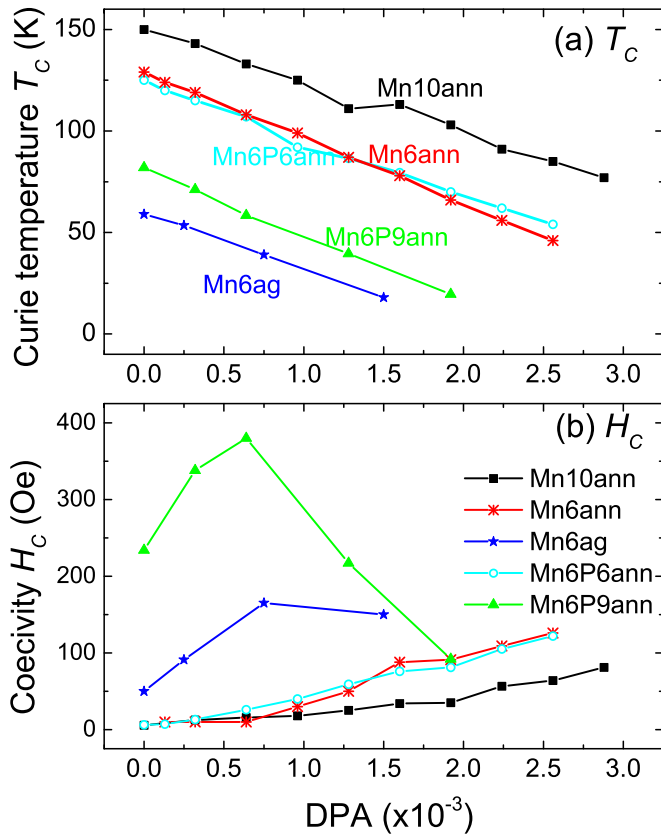
FIG. 2. (a) Curie temperature T_C vs DPA (ion fluence). All samples show a monotonic decrease in T_C. (b) Coercive field H_C vs DPA (ion fluence). For the samples with higher T_C, i.e., less compensation (samples Mn6ann, Mn10ann, and Mn6P6ann), H_C shows a monotonic increase with decreasing hole concentration.

(out-of-plane). Figure 2 shows the Curie temperature T_C and the coercive field H_C as functions of DPA for all samples. Several features can be observed, which will be discussed in detail below. (1) T_C monotonically decreases with increasing compensation of holes by ion irradiation over a broad range of DPA. (2) The shape of magnetization versus temperature remains convex from above. (3) There is no significant difference between the behavior of samples Mn6ann and Mn6P6ann even though the sample Mn6P6ann contains 6% P.

A. T_C versus compensation

Let us first discuss the plausible picture regarding the hole compensation in our samples. We define p as the absolute hole concentration and f as the ratio between the hole and Mn concentrations, $f = 0, 0.5, 1$ meaning full, half, and zero compensation, respectively. The samples Mn6ann, Mn10ann, and Mn6P6ann show rather high T_C and are only weakly compensated by Mn_I or other defects before irradiation. For samples Mn6ann and Mn6P6ann, p has been carefully measured through the Hall effect, showing that f is definitely above 0.5, see Ref. [54]. Moreover, the saturation magnetization for sample Mn6ann (nonirradiated) is around 3.32 μ_B/Mn. The value is nearly the same as that for state-of-the-art high-quality (Ga,Mn)As [55]. According

to Ref. [55], the hole concentration is nearly the same as the effective Mn concentration, $f \approx 1$. The impurity-band picture naturally predicts a strong suppression of carrier-mediated ferromagnetism close to $f = 1$, since then the Fermi energy would fall into a band gap, a mobility gap, or at least an energy range of reduced DOS between the valence band and the purported impurity band [3]. Within the impurity-band framework, we should thus see an increase in T_C as the compensation approaches $f \approx 0.5$. Within the mean-field virtual crystal approximation [56], T_C is proportional to the Mn_{Ga} concentration, to $p^{1/3}$, and to the effective mass m^*. If the hole-hole exchange interactions are included, T_C can be slightly enhanced by 10%–20%. Therefore, in the valence-band picture, T_C is expected to decrease with decreasing hole concentration, regardless of the initial compensation. This is indeed what we find: T_C universally decreases with increasing DPA for all samples. In Appendix D, we calculate the hole concentration p for sample Mn6ann by following the approach described in Ref. [40]. Although T_C reveals a linear dependence on $p^{1/3}$, the dependence of T_C on p is insensitive to the exponent 1/3 or 1 in the range of the hole concentration of our samples. Note that the exponent 1/3 only follows for a parabolic dispersion and neglecting disorder [56]. Our argument does not rely on the specific value of the exponent but on the monotonicity.

B. Phosphorus co-alloying

Phosphorus co-alloying in (Ga,Mn)As has been employed to tune the magnetic anisotropy [57–60], the Fermi energy [61], and the spin stiffness [62]. It is instructive to consider samples Mn6P6ann and Mn6P9ann, which are co-alloyed with 6% and 9% phosphorus, respectively. In the nonirradiated samples, we do not see significant differences in magnetization and T_C between samples Mn6P6ann and Mn6ann, which contains the same nominal concentration of Mn but no P. This strongly differs from the work by Stone *et al.* [63], who observed a significant reduction of T_C upon P co-alloying. They also found that ferromagnetic $Ga_{0.954}Mn_{0.046}As$ films are changed from metallic to insulating by around 2.4% P co-alloying, which is attributed to the fact that holes located within an impurity band are scattered by alloy disorder in the anion sublattice [63]. However, our P-alloyed sample Mn6P6ann is metallic even though the P concentration is 6%. Moreover, comparing samples Mn6ann with Mn6P6ann, our results reveal similar dependence of magnetization and T_C on the hole compensation. On the other hand, sample Mn6P9ann exhibits a remarkable reduction in T_C compared to samples Mn6ann and Mn6P6ann, likely due to its larger concentration of P. In the work by Cubukcu *et al.* [61], the energy level of Mn moves deeper into the gap and the transport character changes from metallic to insulating with increasing P concentration. The Curie temperature drops sharply from 130 to 45 K when the P concentration is increased from 0 to around 19%. The extreme representatives are (Ga,Mn)P and (In,Mn)P, in which the Mn energy levels are located 400 and 220 meV above the valence-band edge, respectively, compared to 110 meV for (Ga,Mn)As. Both materials exhibit hopping conduction [64,65].

A theoretical work by R. Bouzerar *et al.* [66] explains the large reduction of T_C for P co-alloyed (Ga,Mn)As reported in Ref. [63]. They employ the local spin-density approximation to obtain Mn-Mn exchange interactions. These interactions are used in a Heisenberg model with random Mn positions, which is treated by the self-consistent random-phase approximation [67] and complementary Monte Carlo simulations. Compensating defects—P antisites as well as Mn and P interstitials—lead to the reduction of the hole concentration and of T_C compared to (Ga,Mn)As not containing P. If compensating defects can be avoided, the change in T_C is expected to be negligible for low P concentration [61,68], which is indeed in good agreement with our MBE-grown samples.

C. Magnetization and coercivity vs compensation

The reduction of the remanent magnetization M at low temperatures, shown in Fig. 1, is still puzzling. It cannot be explained by a loss of substitutional Mn ions. Note that we applied He-ion irradiation with very low fluences (10^{12}–10^{13} cm^{-2}). The maximal DPA is only 0.2%–0.3% according to SRIM simulations [50]. Most of the substitutional Mn ions are expected to remain at their original sites, as we do not see any change in the channeling analysis along GaAs[001] or [110], see Appendix B. Therefore, within the valence-band framework the magnetization at zero temperature for the compensated samples is expected to stay the same as for the initial sample. Yet we see a significant reduction in both the remanent and the low-temperature saturation magnetization. At the largest fluence applied to sample Mn6ann, see Fig. 1(b), the magnetization is reduced by more than 50%. The reduction of magnetization has been also observed in hydrogenated (Ga,Mn)As with reduced hole concentration [37] and can be reversed by annealing [38]. This phenomenon can be understood by considering the inhomogeneity of (Ga,Mn)As as suggested by Dietl [69] and by Sawicki *et al.* [25]. Carrier-mediated ferromagnetism is strongly influenced by the vicinity of the insulator-to-metal transition (IMT). Particularly, the spatial fluctuations in the local DOS can destroy the spatial homogeneity of the ferromagnetic order, resulting in a nanoscale phase separation. We consider a similar scenario: when defects are introduced, regions with an initially small hole concentration are depleted first and become paramagnetic or superparamagnetic. Therefore a nanoscale phase separation regarding both the effective Mn concentration and the hole concentration can lead to the gradual appearance of superparamagnetic and paramagnetic regions, consequently reducing the total magnetization. Indeed, we have observed a superparamagnetic component in sample Mn6ag with the lowest initial T_C after irradiation up to large He fluences by measuring the zero-field-cooled/field-cooled temperature-dependent magnetization (see Appendix C).

Another reason for a decrease in the magnetization is the occurrence of antiferromagnetically coupled nearest-neighbor Mn_{Ga} pairs when the sample is heavily compensated [56,70]. The antiferromagnetically coupled pairs are invisible in the magnetization even at larger fields since the short-range antiferromagnetic interaction is large compared to the Zeeman energy.

The reduction of the remanent and apparent saturation magnetization with hole compensation naturally leads to an increase in the coercive field H_C. A consistent increase in H_C with DPA for samples Mn6ann, Mn10ann, and Mn6P6ann is indeed seen in Fig. 2. The increase in H_C agrees with predictions obtained from a valence-band description [71], lending additional support to this picture. Note that H_C starts to decrease for samples Mn6P9ann and Mn6ag when the samples are subjected to much larger DPA. It is due to the fact that T_C for those samples are already very low and only slightly above 5 K, the measurement temperature for H_C shown in Fig. 2. On the other hand, the magnetic anisotropy can also change when the compensation is high [37,38,42]. In hydrogenation-compensated (Ga,Mn)As, the coercivity for magnetic field in the in-plane direction also increases [38].

D. Resistivity versus compensation

Corresponding effects are observed in the temperature-dependent resistivity, as shown in Fig. 3. We present data
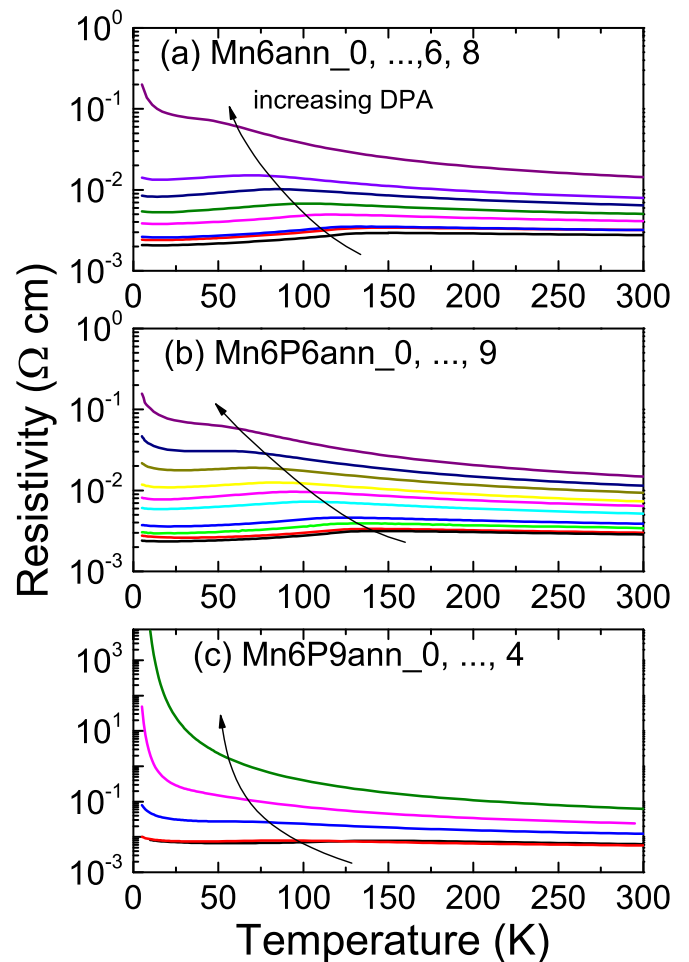

FIG. 3. Temperature-dependent resistivity in zero field for three samples upon ion irradiation. For samples Mn6ann (a) and Mn6P6ann (b), the resistivity continuously increases with decreasing hole concentration but still shows a broadened cusp around T_C, while sample Mn6P9ann (c) is closer to the insulating regime. The arrows indicate the increase of the DPA from 0 to 2.88×10^{-3}. The corresponding DPA values are shown in Fig. 2.

for three samples: Mn6ann, Mn6P6ann, and Mn6P9ann. Mn6P9ann is closer to the insulating regime due to the high concentration of P. With increasing compensation, the resistivity for samples Mn6ann and Mn6P6ann continuously increases and develops an upturn at low temperatures, but both samples still show a broadened cusp around the Curie temperature. For sample Mn6P9ann, the cusp is present for low ion fluence but is overwhelmed by a huge low-temperature increase of the resistivity for moderate fluences. Note the very different relative change of the resistivity value at low temperatures: for samples Mn6ann and Mn6P6ann it changes by less than two orders of magnitude, whereas for sample Mn6P9ann it changes by more than five orders of magnitude. We have also measured the Hall resistance at 300 K (above T_C) for our samples, examples are shown in Appendix D. After irradiation, all samples still show p-type conductivity. The Hall coefficient at 300 K increases gradually with increasing DPA, see Fig. 9 in Appendix D. The results indicate a decrease of the hole concentration, but do not give an accurate measurement due to the paramagnetic component in the Hall effect [54]. However, Mayer *et al.* [40] have used electrochemical capacitance voltage profiling to measure the hole concentration and have confirmed a linear correlation between hole concentration and DPA. We conclude that the moderate increase of resistivity in sample Mn6P6ann is mainly due to the reduction of the free hole concentration, while only at low temperatures an upturn due to carrier localization develops. On the other hand, the large resistivity increase for sample Mn6P9ann with a low initial T_C is dominated by localization.

E. Onset of ferromagnetism

Within the Zener p-d exchange scenario, the Curie temperature should continuously decrease with decreasing hole concentration even into the insulating regime, since the electronic properties at the length scale of the typical Mn-Mn separation change continuously with hole concentration through the IMT [3,25,31]. Actually, Curie temperatures as low as 0.75 K to 2.4 K for p-doped (Zn,Mn)Te [72] and from 5 to 8 K for (In,Mn)Sb [73] were measured.

Within the impurity-band picture [46], the interaction between Mn ions is double-exchange via the hopping of holes between two Mn ions. Therefore the free-hole concentration p has only a weak effect on T_C. Instead, the hopping energy should be a good predictor for ferromagnetism [46]. However, while the experimental data [46] show that ferromagnetic order only occurs within a certain range of hopping energies, the correlation between T_C and the hopping energy is weak. The theory framework described in Ref. [46] predicts a discontinuous disappearance of the ferromagnetic state. Indeed, the experimental T_C for (Ga,Mn)As is reported to jump from 10–15 K to zero.

The Anderson-Mott IMT occurs at a critical carrier concentration p_c. Empirically, the magnitude of p_c is in the range $p_c^{1/3} a_B = 0.26 \pm 0.05$ [1], where a_B is the effective Bohr radius. a_B can be evaluated from the impurity binding energy E_I by $a_B = \hbar/(2m^* E_I)^{1/2}$ or $a_B = e^2/8\pi\epsilon_0\epsilon_r E_I$ [1,74]. For details, see Ref. [1]. For GaAs, the Mn single-impurity binding energy is 110 meV, but for InSb it is as low as several meV. Therefore one can expect a much larger p_c for (Ga,Mn)As than

for (In,Mn)Sb. The double role of Mn ions in GaAs as both local spins and acceptors usually prevents fine tuning of the carrier concentration near the IMT. This may explain the absence of the observation of a continuous decay of T_C to 0 K for (Ga,Mn)As. We expect that a (Ga,Mn)As sample with high Mn concentration but with very low hole concentration shows a T_C close to zero. We choose sample Mn6ag, which has a relatively low initial T_C. Five pieces of sample Mn6ag were irradiated with He ions. The ion fluence was increased in very small step starting from a DPA of 1.5×10^{-3} shown in Fig. 2(a), which leads to the hole concentration decreasing in small steps. Figure 4 shows the magnetic and transport properties of this set of samples. For all of them, the temperature-dependent remanent magnetization is *concave* from above, distinct from Fig. 1. This is typical for DFS with Fermi energy deep in the localized states in the disorder-induced band tail [75]. For these concave magnetization curves, it is difficult to extract precise values for T_C. Nevertheless, T_C in the range 5–10 K is observed. It is more instructive to consider the magnetization in field measured at 2 K, shown in Fig. 4(b). The samples still show clear ferromagnetic hysteresis and the saturation magnetization decreases gradually with increasing DPA. This is consistent with the suppression of ferromagnetism with decreasing hole concentration. We note that this set of samples all show insulating behavior, consistent with strong disorder. The conductivity can be understood as hopping as shown in Figs. 4(c) and 4(d) by fitting to a $T^{-0.5}$ dependence [76].

Our results provide direct experimental evidence that ferromagnetism can be suppressed with T_C below 10 K by introducing hole compensation in (Ga,Mn)As samples with large Mn concentration. This is easy to understand within the valence-band picture. In sample Mn6ag with $x = 0.06$, the Mn-derived impurity band is merged with the valence band before we introduce hole compensation. If we introduce compensation, the Fermi energy shifts up into the tail of the valence band. With decreasing hole concentration, the Fermi energy shifts deeper and deeper into this tail. States at the Fermi energy are thus more and more localized. Ferromagnetism is mainly determined by the properties of the hole states on the length scale of the typical Mn-Mn nearest-neighbor distance, which change smoothly with the localization length and thus with compensation. Since the Mn concentration is high, the Mn-Mn distance is typically smaller than the effective Bohr radius of an acceptor-bound state. In this sense, the Zener p-d exchange can still happen, leading to the formation of Zhang-Rice magnetic polarons [77,78]. The temperature below which the magnetic polarons overlap and ferromagnetic order develops depends on the hole concentration. Consequently, T_C can be decreased to close to zero Kelvin when the hole concentration is gradually reduced.

IV. SUMMARY AND CONCLUSIONS

We have presented the magnetic and transport properties of a broad range of (Ga,Mn)As-based DFS samples. The DFS samples used in this study are of state-of-the-art quality, as shown by their high T_C and confirmed by x-ray diffraction measurements [54,79]. We have observed a monotonic decrease of T_C with decreasing hole concentration over a large temperature range and the existence of Curie temperatures
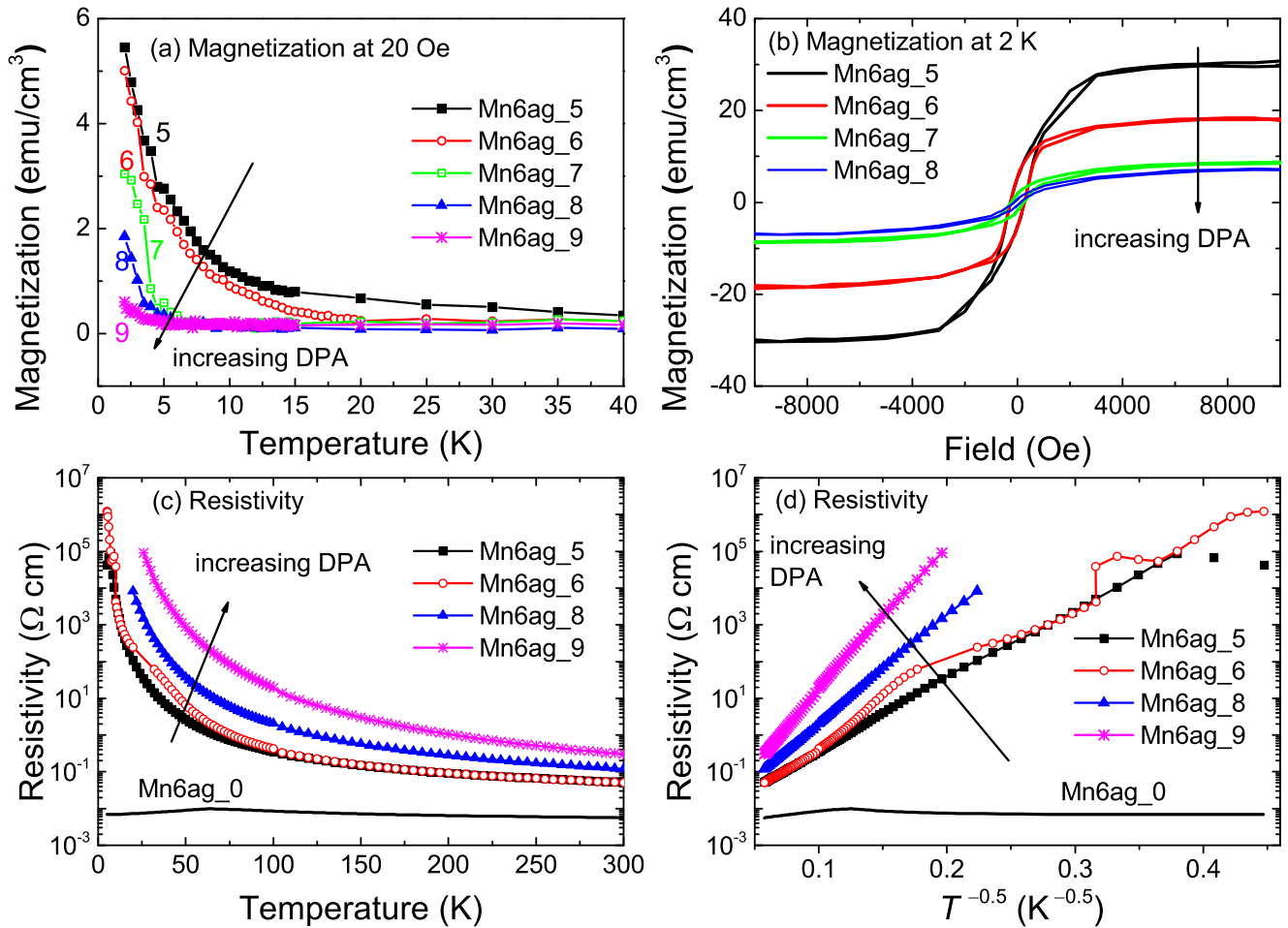
FIG. 4. Change of magnetic and transport properties of sample Mn6ag with compensation, close to the destruction of ferromagnetism. (a) Temperature dependent magnetization in a field of 20 Oe, (b) Magnetization vs field at 2 K. (c) and (d) temperature-dependent longitudinal resistance in zero field. A virgin, nonirradiated sample (Mn6ag_0) is shown for comparison. Mn6ag_5, . . . , Mn6ag_9 label the samples with different DPA.

below 10 K for heavily compensated samples. These observations cannot be explained if there is a pronounced dip in the DOS between the Mn impurity derived state and the GaAs valence band. Our results rather support the valence-band picture for high-quality (Ga,Mn)As-based DFS. But how can we then understand the experimental results reported in Refs. [27,40,41,63], which are not consistent with the valence-band picture? We first note that in Refs. [27,40,41], the total Mn concentrations are 5%, 4.5%, and 6.8%, but the corresponding T_C is only around 60, 80, and 90 K, respectively. This means that the starting materials were already highly compensated by defects. The large influence of a small concentration of P reported in Ref. [63] was later explained by the presence of additional defects arising with P co-alloying by ion implantation and pulsed laser annealing [66]. Given the fact that the preparation of ferromagnetic (Ga,Mn)As is a rather delicate procedure, a small deviation in growth parameters can significantly alter the properties of the prepared materials [32]. A reliable conclusion can only be obtained by working with highest-quality (Ga,Mn)As materials [80].

Finally, we return to the question alluded to in the beginning: is there hope to realize DFS with T_C above room temperature? Within the valence-band picture with p-d

exchange, based on the present results, we suggest to search for materials (a) with smaller lattice constants, which lead to a larger p-d exchange [3] and (b) with a large concentration of mobile holes. The criterion (a) is usually positively correlated with a wide bandgap of the host semiconductor. For Mn in III-V semiconductors, unfortunately, the two criteria cannot be fulfilled simultaneously, since the p-d hybridization increases the binding energy of Mn acceptors going from arsenides to phosphides and finally nitrides. In samples with strong p-d hybridization, the holes are more localized. Moreover, it is generally difficult to achieve p-type doping in wide-band-gap semiconductors, particularly in GaN and ZnO [81,82], even by doping with shallower acceptors than Mn. Searching for different transition-metal dopants is less promising, since other transition-metal ions substituted for the cation tend to have several energy levels of both donor and acceptor type. It has turned out that up to now (Ga,Mn)As yields the best compromise and has achieved the highest T_C [3,83,84]. Nevertheless, an intentional introduction of nanoscale inhomogeneities has been proposed as a path to achieve high Curie temperatures in diluted systems [85–87]. Moreover, Mn-doped I-II-V compounds [88] with decoupled spin and charge doping might provide an alternative test bed for producing DFS

with high T_C. At the present stage, T_C reaches 220 K in $(Ba_{0.7}K_{0.3})(Zn_{0.85}Mn_{0.15})_2As_2$ [89].

TABLE II. Sample notations, energy, and fluence of He ions.

Samples	Energy	Fluence (cm^{-2})	Peak DPA
Mn6ann_0	–	0	0
Mn6ann_1	4 keV	2.0×10^{12}	0.13×10^{-3}
Mn6ann_2	4 keV	5.0×10^{12}	0.32×10^{-3}
Mn6ann_3	4 keV	1.0×10^{13}	0.64×10^{-3}
Mn6ann_4	4 keV	1.5×10^{13}	0.96×10^{-3}
Mn6ann_5	4 keV	2.0×10^{13}	1.28×10^{-3}
Mn6ann_6	4 keV	2.5×10^{13}	1.60×10^{-3}
Mn6ann_7	4 keV	3.0×10^{13}	1.92×10^{-3}
Mn6ann_8	4 keV	3.5×10^{13}	2.24×10^{-3}
Mn6ann_9	4 keV	4.0×10^{13}	2.56×10^{-3}
Mn6ag_0	–	0	0
Mn6ag_1	650 keV	1.0×10^{14}	0.25×10^{-3}
Mn6ag_2	650 keV	3.0×10^{14}	0.75×10^{-3}
Mn6ag_3	650 keV	6.0×10^{14}	1.50×10^{-3}
Mn6ag_4	650 keV	10.0×10^{14}	2.50×10^{-3}
Mn6ag_5	4 keV	2.0×10^{13}	1.28×10^{-3}
Mn6ag_6	4 keV	2.5×10^{13}	1.60×10^{-3}
Mn6ag_7	4 keV	3.0×10^{13}	1.92×10^{-3}
Mn6ag_8	4 keV	3.5×10^{13}	2.24×10^{-3}
Mn6ag_9	4 keV	4.0×10^{13}	2.56×10^{-3}
Mn10ann_0	–	0	0
Mn10ann_1	4 keV	5.0×10^{12}	0.32×10^{-3}
Mn10ann_2	4 keV	1.0×10^{13}	0.64×10^{-3}
Mn10ann_3	4 keV	1.5×10^{13}	0.96×10^{-3}
Mn10ann_4	4 keV	2.0×10^{13}	1.28×10^{-3}
Mn10ann_5	4 keV	2.5×10^{13}	1.60×10^{-3}
Mn10ann_6	4 keV	3.0×10^{13}	1.92×10^{-3}
Mn10ann_7	4 keV	3.5×10^{13}	2.24×10^{-3}
Mn10ann_8	4 keV	4.0×10^{13}	2.56×10^{-3}
Mn10ann_9	4 keV	4.5×10^{13}	2.88×10^{-3}
Mn6P6ann_0	–	0	0
Mn6P6ann_1	4 keV	2.0×10^{12}	0.13×10^{-3}
Mn6P6ann_2	4 keV	5.0×10^{12}	0.32×10^{-3}
Mn6P6ann_3	4 keV	1.0×10^{13}	0.64×10^{-3}
Mn6P6ann_4	4 keV	1.5×10^{13}	0.96×10^{-3}
Mn6P6ann_5	4 keV	2.0×10^{13}	1.28×10^{-3}
Mn6P6ann_6	4 keV	2.5×10^{13}	1.60×10^{-3}
Mn6P6ann_7	4 keV	3.0×10^{13}	1.92×10^{-3}
Mn6P6ann_8	4 keV	3.5×10^{13}	2.24×10^{-3}
Mn6P6ann_9	4 keV	4.0×10^{13}	2.56×10^{-3}
Mn6P9ann_0	–	0	0
Mn6P9ann_1	4 keV	5.0×10^{12}	0.32×10^{-3}
Mn6P9ann_2	4 keV	1.0×10^{13}	0.64×10^{-3}
Mn6P9ann_3	4 keV	2.0×10^{13}	1.28×10^{-3}
Mn6P9ann_4	4 keV	3.0×10^{13}	2.56×10^{-3}

The samples listed in Table I were irradiated with He ions. The sample notation and experimental condition are listed in Table II.

APPENDIX B: RUTHERFORD BACKSCATTERING SPECTROMETRY/CHANNELING

Rutherford backscattering spectrometry/channeling (RBS) is sensitive to the crystalline disorder and is able to quantitatively measure the fraction of substitutional and interstitial Mn ions [51,53]. Since the interstitial Mn ions can be invisible along GaAs[001] [51,53], we measure the channeling spectra along both GaAs[001] and [110] axis. The RBS measurements were performed with a collimated 1.7 MeV He$^+$ beam at a backscattering angle of 170°. The sample was mounted on a three-axis goniometer with a precision of 0.01°. The channeling spectra were measured by aligning the samples to make the impinging He$^+$ beam parallel to the GaAs[001] or [110] axis. Figure 5 shows a measurement for samples Mn6ann before and after ion irradiation (up to the largest He ion fluence). Within the detection limit, there is no signature of an increase in the number of interstitial Mn ions. In Fig. 5(b), the expected channeling spectrum [53] in the presence of interstitial Mn ions is schematically drawn on top of the experiment spectrum.
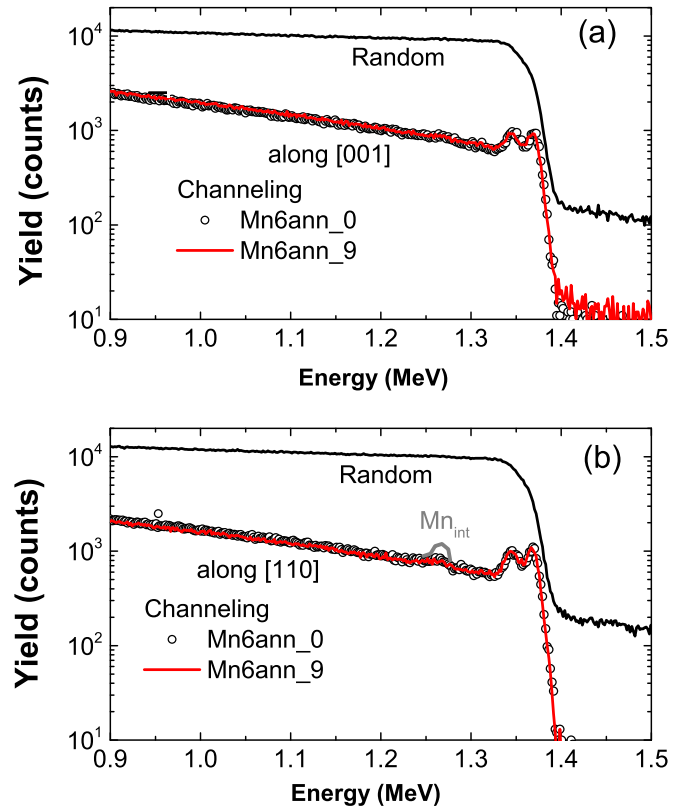

FIG. 5. RBS/Channeling results for sample Mn6ann, comparing virgin (Mn6ann_0) and irradiated (Mn6ann_9) samples. The channeling spectra do not reveal any detectable increase in yield along both [001] (a) and [110] (b). The grey curve schematically drawn in (b) indicates the expected spectrum if there is a lot of Mn interstitials after irradiation.
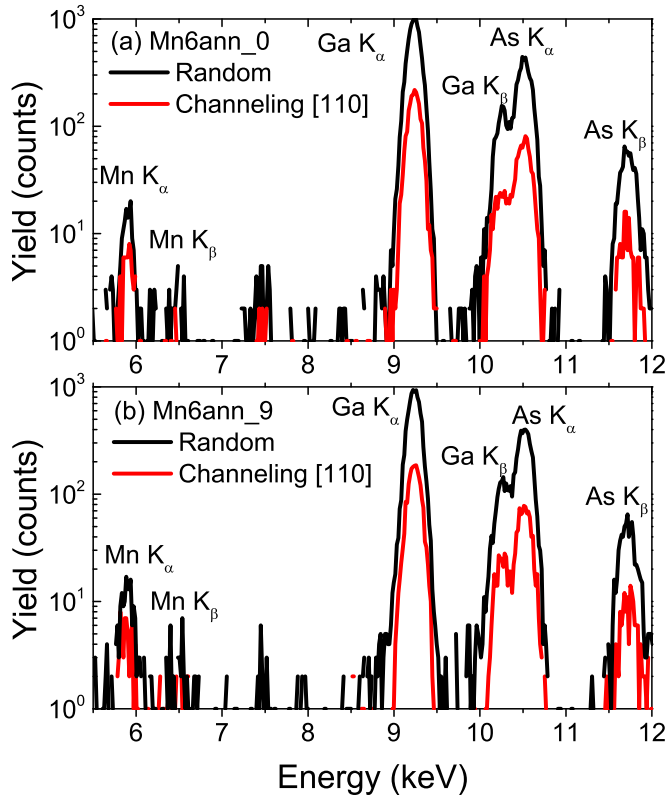
FIG. 6. PIXE/Channeling results for sample Mn6ann along GaAs[110]: (a) Mn6ann_0 before irradiation and (b) Mn6ann_9 after irradiation with largest fluence. In both samples, the channeling effect is clearly revealed.

Moreover, the particle-induced x-ray emission (PIXE) was recorded simultaneously during RBS measurements. The advantage is that the Mn K lines are well separated from the Ga and As K lines. However, the emission is relatively weak since we use He ions instead of proton [51]. Figure 6 shows the PIXE/channeling spectra along GaAs[110] for both samples Mn6ann_0 and Mn6ann_9. Although the signal from Mn K-lines is weak and noisy, the channeling effect is clearly revealed: the emission is much dropped when the beam is along GaAs[110] (the red spectra in the figure). One can roughly estimate the nonrandom fraction (f_{nr}) of Mn using $f_{nr} = (1 - \chi_{Mn}/(1 - \chi_{Ga})$. Here, χ_{Mn} (χ_{Ga}) is the ratio between the integral intensity of the Mn K_{α} (Ga K_{α}) at the channeling geometry and at the random geometry. For both samples, f_{nr} is estimated to be around 75%. This number can be considered as a measure of the substitutional fraction of Mn. However, f_{nr} can be smaller than the Mn substitutional fraction due to the flux peaking effect [51,53]. Nevertheless, f_{nr} along GaAs[110] remains the same after He ion irradiation up to the largest fluence.

APPENDIX C: SUPERPARAMAGNETISM IN HIGHLY COMPENSATED (Ga,Mn)As

As noted in Sec. III C, carrier-mediated ferromagnetism is strongly influenced by the vicinity of the IMT. In particular, spatial fluctuations in the effective Mn and hole concentrations are expected to lead to the formation of paramagnetic

or superparamagnetic regions, as the hole concentration is reduced. We have indeed observed signatures for paramagnetic and superparamagnetic components in sample Mn6ag after irradiation.

The appearance of a superparamagnetic component is demonstrated by measuring the zero-field-cooled/field-cooled (ZFC/FC) temperature-dependent magnetization for sample Mn6ag_3, which is heavily compensated but still shows magnetic hysteresis. In the ZFC measurement, the sample was cooled down from around 300 to 5 K in zero field. Then a small field (in this work 20, 50, 100, and 200 Oe, respectively) was applied. The magnetization was measured during warming up to 300 K. Then the field was kept and the sample was cooled from 300 to 5 K. During cooling, the FC magnetization was
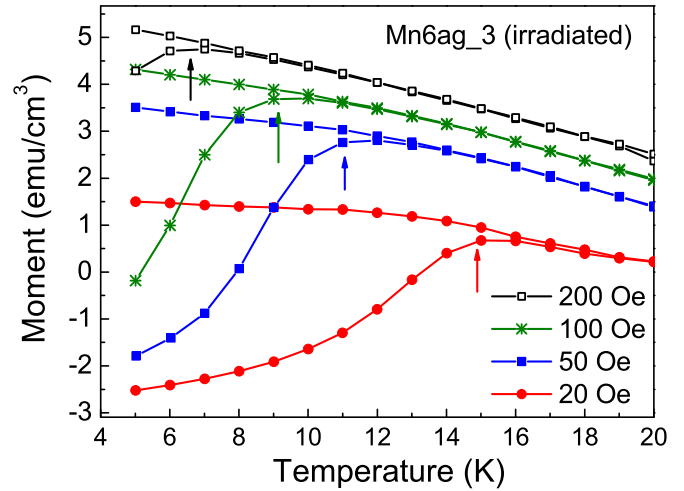

FIG. 7. ZFC/FC magnetization curves for the sample Mn6ag after irradiation. The measurements were performed in different fields. The curves are vertically shifted for better visibility. The disparity between the ZFC and FC curves is the signature of superparamagnetism. The blocking temperatures (indicated by arrows) are shifted to lower temperatures with increasing measurement field.
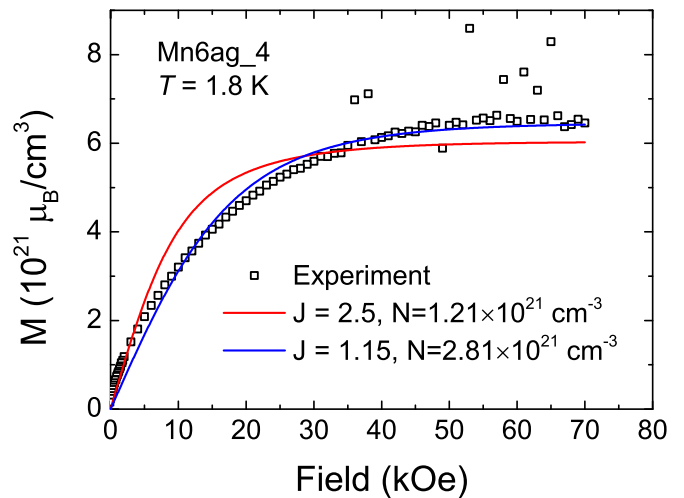

FIG. 8. Magnetization measured at 1.8 K for sample Mn6ag_4 (the most highly compensated sample). The diamagnetic background has been subtracted. The solid lines are fits using the Brillouin function. The fitting results are also shown in the figure.

recorded. A similar approach was used in Ref. [25]. If there is a superparamagnetic component, one expects to observe a difference between the ZFC and FC curves, as is indeed found in Fig. 7. The maximum in ZFC magnetization occurs at the so-called blocking temperature, which depends on the size of superparamagnetic particles and on the external field. For larger external field, the single-domain superparamagnetic clusters can flip into the field direction at lower temperature. In our measurement, the blocking temperature decreases as the external field is increased from 20 to 200 Oe.

Figure 8 shows the magnetization for sample Mn6ag_4 measured at 1.8 K after subtracting the diamagnetic background. This sample does not show any ferromagnetic hysteresis down to 1.8 K. At 1.8 K, the magnetization does not show saturation up to a field of 7 T. We fit the magnetization by a Brillouin function,

$$M(\alpha) = N J \mu_B g \left[\frac{2J+1}{2J} \coth \left(\frac{2J+1}{2J} \alpha \right) \right.$$
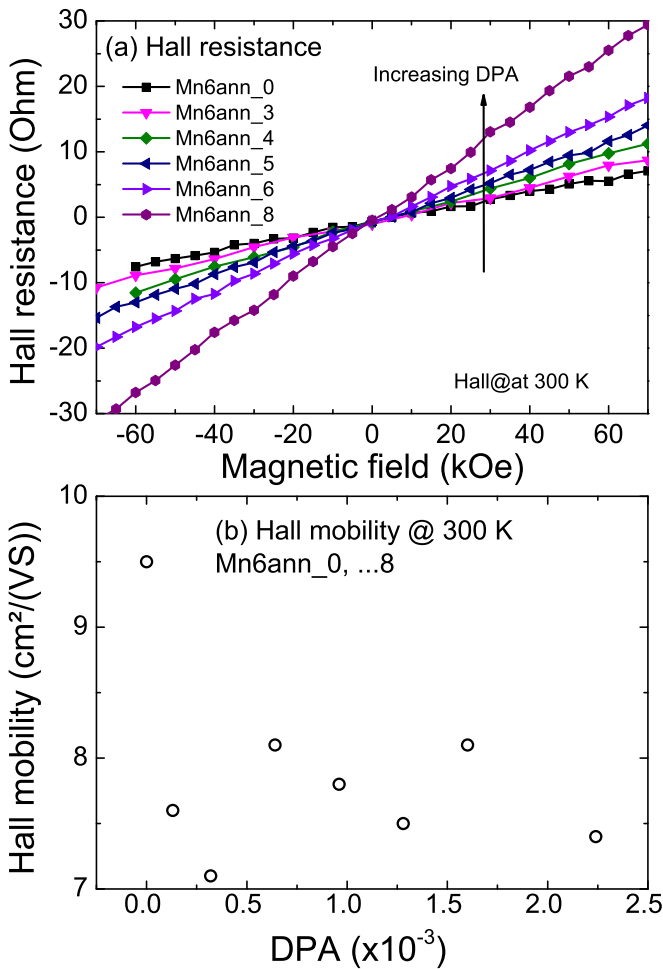$$\left. - \frac{1}{2J} \coth \left(\frac{\alpha}{2J} \right) \right], \tag{C1}$$

FIG. 9. (a) Hall resistance vs applied field measured for several samples from Mn6ann after irradiation and (b) Hall mobility for the same set of samples. All samples show *p*-type conductivity and the hole concentration decreases gradually. The Hall mobility decreases after irradiation but remains rather independent of DPA.

where the *g* factor is about 2 if assuming Mn^{2+} (d^5) without holes [90,91], μ_B is the Bohr magneton, $\alpha = g J \mu_B H / k_B T$, k_B is the Boltzmann constant, and *N* is the density of spins.

As shown in Fig. 8, the fit for fixed $J = 2.5$ does not well reproduce the experimental data. A better fit is obtained for $J = 1.15$. This can be explained by considering another component of paramagnetism arising from intrinsic defects in the GaAs substrate [92], which technically cannot be subtracted from the magnetization measurement since the defect concentration can be different depending on the growth condition. This component can be represented by spin 1/2 ($J = S = 0.5$) paramagnetism. Moreover, the other states of Mn impurities could have different *g* factor and *J* value [91]. Therefore it is difficult to accurately separate different paramagnetic components and is beyond the scope of this paper. Nevertheless, a fully compensated (Ga,Mn)As sample shows paramagnetic behavior.

APPENDIX D: HOLE CONCENTRATION

Figure 9(a) shows the Hall resistance measured at 300 K for sample Mn6ann. For increasing DPA, the samples remain p-type conducting, but the Hall resistance increases, indicating a decrease of the hole concentration. Estimated from the Hall measurement shown in Fig. 9(a), the hole concentration gradually decreases from around 2.6×10^{20} cm^{-3} for the virgin sample to 5.6×10^{19} cm^{-3} for sample
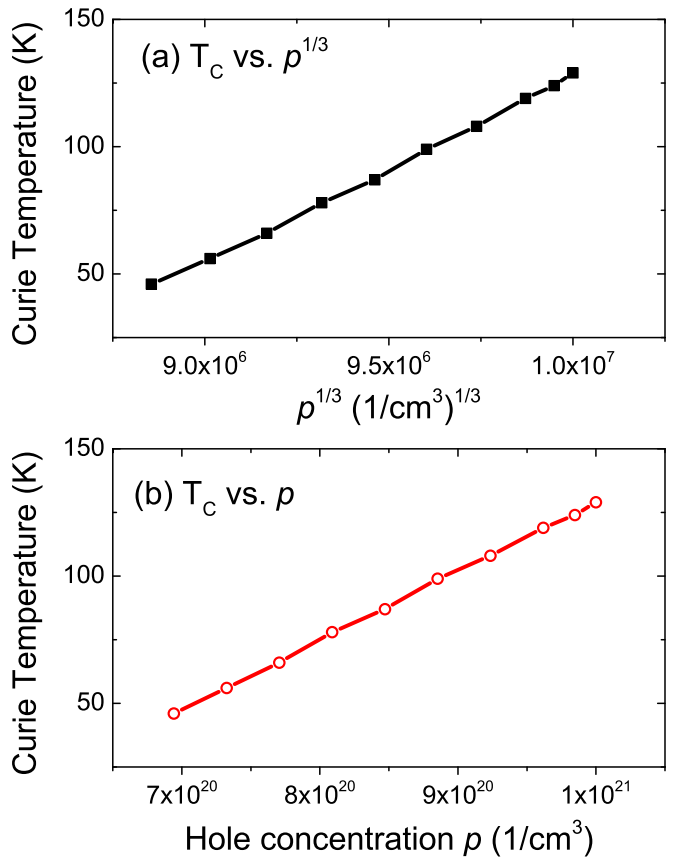

FIG. 10. Curie temperature vs hole concentration *p*: (a) $p^{1/3}$ and (b) *p* for samples Mn6ann_0,9. The hole concentration is estimated by following the approach in Ref. [40].

Mn6ann_8. However, due to the paramagnetic component in the Hall resistance [54], the hole concentration is significantly underestimated. We have also estimated the Hall mobility, which decreases after irradiation but remains rather independent of DPA, see Fig. 9(b). However, one has to note the possible overestimation of the Hall mobility due to the underestimated hole concentration.

The initial hole concentration is around 1×10^{21} cm^{-3}, which has been measured by the sample preparation group at low temperature and high field on a similar sample [54]. This value can also be confirmed from our PIXE/channeling measurement. If we assume the nonrandom Mn fraction as the substitutional fraction (75%) and most compensating Mn

interstitials have been kicked out during the postgrowth, long-time low-temperature annealing, the hole concentration is 2.21×10^{22} cm$^{-3} \times 0.06 \times 0.75 = 0.99 \times 10^{21}$ cm^{-3}. The hole compensation rate by ion irradiation is estimated to be 0.91 hole per vacancy [40]. Then we can calculate the hole concentration p for sample Mn6ann after irradiation and plot T_C vs $p^{1/3}$ as shown in Fig. 10. As one can see, T_C reveals a linear dependence on $p^{1/3}$. However, the dependence is not sensitive to the exponent 1/3 or 1 in the range of the hole concentration of our samples. Note that the exponent 1/3 only follows for a parabolic dispersion and neglecting disorder [56]. Our argument does not rely on the specific value of the exponent but on the monotonicity.

[1] T. Dietl and H. Ohno, Rev. Mod. Phys. **86**, 187 (2014).

[2] T. Jungwirth, J. Sinova, J. Mašek, J. Kučera, and A. H. MacDonald, Rev. Mod. Phys. **78**, 809 (2006).

[3] T. Dietl, Nat. Mater. **9**, 965 (2010).

[4] C. Timm, in *Handbook of Spin Transport and Magnetism*, edited by E. Y. Tsymbal and I. Žutić (CRC Press, Boca Raton, FL, 2012), p. 385.

[5] G. Bouzerar and R. Bouzerar, C. R. Phys. **16**, 731 (2015).

[6] Y. Ohno, D. K. Young, B. Beschoten, F. Matsukura, H. Ohno, and D. D. Awschalom, Nature (London) **402**, 790 (1999).

[7] D. Chiba, M. Yamanouchi, F. Matsukura, and H. Ohno, Science **301**, 943 (2003).

[8] M. Ciorga, M. Schlapps, A. Einwanger, S. Geißler, J. Sadowski, W. Wegscheider, and D. Weiss, New J. Phys. **9**, 351 (2007).

[9] M. Ciorga, A. Einwanger, U. Wurstbauer, D. Schuh, W. Wegscheider, and D. Weiss, Phys. Rev. B **79**, 165321 (2009).

[10] I. Stolichnov, S. W. E. Riester, H. J. Trodahl, N. Setter, A. W. Rushforth, K. W. Edmonds, R. P. Campion, C. T. Foxon, B. L. Gallagher, and T. Jungwirth, Nat. Mater. **7**, 464 (2008).

[11] V. L. Korenev, I. A. Akimov, S. V. Zaitsev, V. F. Sapega, L. Langer, D. R. Yakovlev, Y. A. Danilov, and M. Bayer, Nat. Commun. **3**, 959 (2012).

[12] L. Vila, R. Giraud, L. Thevenard, A. Lemaître, F. Pierre, J. Dufouleur, D. Mailly, B. Barbara, and G. Faini, Phys. Rev. Lett. **98**, 027204 (2007).

[13] B. Endres, M. Ciorga, M. Schmid, M. Utz, D. Bougeard, D. Weiss, G. Bayreuther, and C. H. Back, Nat. commun. **4**, 2068 (2013).

[14] J. Gorchon, J. Curiale, A. Lemaître, N. Moisan, M. Cubukcu, G. Malinowski, C. Ulysse, G. Faini, H. J. von Bardeleben, and V. Jeudy, Phys. Rev. Lett. **112**, 026601 (2014).

[15] L. Chen, X. Yang, F. Yang, J. Zhao, J. Misuraca, P. Xiong, and S. von Molnar, Nano Lett. **11**, 2584 (2011).

[16] A. Zunger, in *Solid State Physics Vol. 39*, edited by H. Ehrenreich and D. Turnbull (Academic Press, Orlando, 1986), p. 275.

[17] P. Mahadevan and A. Zunger, Phys. Rev. B **68**, 075202 (2003).

[18] K. S. Burch, D. B. Shrekenhamer, E. J. Singley, J. Stephens, B. L. Sheu, R. K. Kawakami, P. Schiffer, N. Samarth, D. D. Awschalom, and D. N. Basov, Phys. Rev. Lett. **97**, 087208 (2006).

[19] R. Bouzerar, G. Bouzerar, and T. Ziman, Phys. Rev. B **73**, 024411 (2006).

[20] T. Jungwirth, J. Sinova, A. H. MacDonald, B. L. Gallagher, V. Novák, K. W. Edmonds, A. W. Rushforth, R. P. Campion, C. T. Foxon, L. Eaves, E. Olejník, J. Mašek, S.-R. E. Yang, J. Wunderlich, C. Gould, L. W. Molenkamp, T. Dietl, and H. Ohno, Phys. Rev. B **76**, 125206 (2007).

[21] E. J. Singley, R. Kawakami, D. D. Awschalom, and D. N. Basov, Phys. Rev. Lett. **89**, 097203 (2002).

[22] B. C. Chapler, R. C. Myers, S. Mack, A. Frenzel, B. C. Pursley, K. S. Burch, E. J. Singley, A. M. Dattelbaum, N. Samarth, D. D. Awschalom, and D. N. Basov, Phys. Rev. B **84**, 081203 (2011).

[23] G. Acbas, M.-H. Kim, M. Cukr, V. Novák, M. A. Scarpulla, O. D. Dubon, T. Jungwirth, J. Sinova, and J. Cerne, Phys. Rev. Lett. **103**, 137201 (2009).

[24] T. Jungwirth, P. Horodyská, N. Tesařová, P. Němec, J. Šubrt, P. Malý, P. Kužel, C. Kadlec, J. Mašek, I. Němec, M. Orlita, V. Novák, K. Olejnik, Z. Šobáň, P. Vašek, P. Svoboda, and J. Sinova, Phys. Rev. Lett. **105**, 227201 (2010).

[25] M. Sawicki, D. Chiba, A. Korbecka, Y. Nishitani, J. A. Majewski, F. Matsukura, T. Dietl, and H. Ohno, Nat. Phys. **6**, 22 (2010).

[26] S. Ohya, K. Takata, and M. Tanaka, Nat. Phys. **7**, 342 (2011).

[27] M. Dobrowolska, K. Tivakornsasithorn, X. Liu, J. K. Furdyna, M. Berciu, K. M. Yu, and W. Walukiewicz, Nat. Mater. **11**, 444 (2012).

[28] N. Samarth, Nat. Mater. **11**, 360 (2012).

[29] S. C. Erwin and A. G. Petukhov, Phys. Rev. Lett. **89**, 227201 (2002).

[30] B. C. Chapler, S. Mack, R. C. Myers, A. Frenzel, B. C. Pursley, K. S. Burch, A. M. Dattelbaum, N. Samarth, D. D. Awschalom, and D. N. Basov, Phys. Rev. B **87**, 205314 (2013).

[31] T. Dietl, H. Ohno, F. Matsukura, J. Cibert, and D. Ferrand, Science **287**, 1019 (2000).

[32] P. Nemec, V. Novak, N. Tesarova, E. Rozkotova, H. Reichlova, D. Butkovicova, F. Trojanek, K. Olejnik, P. Maly, R. P. Campion, B. L. Gallagher, J. Sinova, and T. Jungwirth, Nat. Commun. **4**, 1422 (2013).

[33] G. Bouzerar, T. Ziman, and J. Kudrnovský, Phys. Rev. B **72**, 125207 (2005).

[34] R. C. Myers, B. L. Sheu, A. W. Jackson, A. C. Gossard, P. Schiffer, N. Samarth, and D. D. Awschalom, Phys. Rev. B **74**, 155203 (2006).

[35] S. T. B. Goennenwein, T. A. Wassner, H. Huebl, M. S. Brandt, J. B. Philipp, M. Opel, R. Gross, A. Koeder, W. Schoch, and A. Waag, Phys. Rev. Lett. **92**, 227202 (2004).

[36] L. Thevenard, L. Largeau, O. Mauguin, A. Lemaître, and B. Theys, Appl. Phys. Lett. **87**, 182506 (2005).

[37] K. Khazen, H. J. von Bardeleben, J. L. Cantin, L. Thevenard, L. Largeau, O. Mauguin, and A. Lemaître, Phys. Rev. B **77**, 165204 (2008).

[38] L. Thevenard, L. Largeau, O. Mauguin, A. Lemaître, K. Khazen, and H. J. von Bardeleben, Phys. Rev. B **75**, 195218 (2007).

[39] H. Ohno, D. Chiba, F. Matsukura, T. Omiya, E. Abe, T. Dietl, Y. Ohno, and K. Ohtani, Nature (London) **408**, 944 (2000).

[40] M. A. Mayer, P. R. Stone, N. Miller, H. M. Smith, O. D. Dubon, E. E. Haller, K. M. Yu, W. Walukiewicz, X. Liu, and J. K. Furdyna, Phys. Rev. B **81**, 045205 (2010).

[41] E. H. C. P. Sinnecker, G. M. Penello, T. G. Rappoport, M. M. Sant'Anna, D. E. R. Souza, M. P. Pires, J. K. Furdyna, and X. Liu, Phys. Rev. B **81**, 245203 (2010).

[42] L. Li, S. D. Yao, S. Zhou, D. Bürger, O. Roshchupkina, S. Akhmadaliev, A. W. Rushforth, R. P. Campion, J. Fassbender, M. Helm, B. L. Gallagher, C. Timm, and H. Schmidt, J. Phys. D: Appl. Phys. **44**, 045001 (2011).

[43] S. Pearton, Mater. Sci. Eng. R-Rep. **4**, 313 (1990).

[44] P. N. K. Deenapanray, Q. Gao, and C. Jagadish, J. Appl. Phys. **93**, 9123 (2003).

[45] T. E. Winkler, P. R. Stone, T. Li, K. M. Yu, A. Bonanni, and O. D. Dubon, Appl. Phys. Lett. **98**, 012103 (2011).

[46] B. L. Sheu, R. C. Myers, J.-M. Tang, N. Samarth, D. D. Awschalom, P. Schiffer, and M. E. Flatté, Phys. Rev. Lett. **99**, 227205 (2007).

[47] M. Wang, R. P. Campion, A. W. Rushforth, K. W. Edmonds, C. T. Foxon, and B. L. Gallagher, Appl. Phys. Lett. **93**, 132103 (2008).

[48] R. Campion, K. Edmonds, L. Zhao, K. Wang, C. Foxon, B. Gallagher, and C. Staddon, J. Cryst. Growth **247**, 42 (2003).

[49] L. Chen, S. Yan, P. F. Xu, J. Lu, W. Z. Wang, J. J. Deng, X. Qian, Y. Ji, and J. H. Zhao, Appl. Phys. Lett. **95**, 182505 (2009).

[50] J. Ziegler, J. Biersack, and U. Littmark, *The Stopping and Range of Ions in Solids* (Pergamon Press, New York, 1985).

[51] K. M. Yu, W. Walukiewicz, T. Wojtowicz, I. Kuryliszyn, X. Liu, Y. Sasaki, and J. K. Furdyna, Phys. Rev. B **65**, 201303 (2002).

[52] L. M. C. Pereira, U. Wahl, S. Decoster, J. G. Correia, L. M. Amorim, M. R. da Silva, J. P. Araújo, and A. Vantomme, Phys. Rev. B **86**, 125206 (2012).

[53] D. Benzeggouta, K. Khazen, I. Vickridge, H. J. von Bardeleben, L. Chen, X. Z. Yu, and J. H. Zhao, Phys. Rev. B **89**, 115323 (2014).

[54] M. Wang, Ph.D. thesis, University of Nottingham, 2012.

[55] T. Jungwirth, J. Mašek, K. Y. Wang, K. W. Edmonds, M. Sawicki, M. Polini, J. Sinova, A. H. MacDonald, R. P. Campion, L. X. Zhao, N. R. S. Farley, T. K. Johal, G. van der Laan, C. T. Foxon, and B. L. Gallagher, Phys. Rev. B **73**, 165205 (2006).

[56] T. Jungwirth, K. Y. Wang, J. Mašek, K. W. Edmonds, J. König, J. Sinova, M. Polini, N. A. Goncharuk, A. H. MacDonald, M. Sawicki, A. W. Rushforth, R. P. Campion, L. X. Zhao, C. T. Foxon, and B. L. Gallagher, Phys. Rev. B **72**, 165204 (2005).

[57] A. Lemaître, A. Miard, L. Travers, O. Mauguin, L. Largeau, C. Gourdon, V. Jeudy, M. Tran, and J.-M. George, Appl. Phys. Lett. **93**, 021123 (2008).

[58] M. Cubukcu, H. J. von Bardeleben, K. Khazen, J. L. Cantin, O. Mauguin, L. Largeau, and A. Lemaître, Phys. Rev. B **81**, 041202(R) (2010).

[59] M. Cubukcu, H. J. von Bardeleben, J. L. Cantin, and A. Lemaître, Appl. Phys. Lett. **96**, 102502 (2010).

[60] M. Yahyaoui, K. Boujdaria, M. Cubukcu, C. Testelin, and C. Gourdon, J. Phys.: Conden. Matter **25**, 346001 (2013).

[61] M. Cubukcu, H. von Bardeleben, J. Cantin, I. Vickridge, and A. Lemaitre, Thin Solid Films **519**, 8212 (2011).

[62] S. Shihab, H. Riahi, L. Thevenard, H. J. von Bardeleben, A. Lemaître, and C. Gourdon, Appl. Phys. Lett. **106**, 142408 (2015).

[63] P. R. Stone, K. Alberi, S. K. Z. Tardif, J. W. Beeman, K. M. Yu, W. Walukiewicz, and O. D. Dubon, Phys. Rev. Lett. **101**, 087203 (2008).

[64] M. A. Scarpulla, B. L. Cardozo, R. Farshchi, W. M. H. Oo, M. D. McCluskey, K. M. Yu, and O. D. Dubon, Phys. Rev. Lett. **95**, 207204 (2005).

[65] M. Khalid, E. Weschke, W. Skorupa, M. Helm, and S. Zhou, Phys. Rev. B **89**, 121301 (2014).

[66] R. Bouzerar, F. Máca, J. Kudrnovský, and L. Bergqvist, Phys. Rev. B **82**, 035207 (2010).

[67] G. Bouzerar, T. Ziman, and J. Kudrnovský, Europhys. Lett. **69**, 812 (2005).

[68] A. W. Rushforth, M. Wang, N. R. S. Farley, R. P. Campion, K. W. Edmonds, C. R. Staddon, C. T. Foxon, and B. L. Gallagher, J. Appl. Phys. **104**, 073908 (2008).

[69] T. Dietl, J. Phys. Soc. Jpn. **77**, 031005 (2008).

[70] J. Kudrnovský, I. Turek, V. Drchal, F. Máca, P. Weinberger, and P. Bruno, Phys. Rev. B **69**, 115208 (2004).

[71] M. Abolfath, T. Jungwirth, J. Brum, and A. H. MacDonald, Phys. Rev. B **63**, 054418 (2001).

[72] D. Ferrand, J. Cibert, A. Wasiela, C. Bourgognon, S. Tatarenko, G. Fishman, T. Andrearczyk, J. Jaroszyński, S. Koleśnik, T. Dietl, B. Barbara, and D. Dufeu, Phys. Rev. B **63**, 085201 (2001).

[73] T. Wojtowicz, G. Cywiński, W. L. Lim, X. Liu, M. Dobrowolska, J. K. Furdyna, K. M. Yu, W. Walukiewicz, G. B. Kim, M. Cheon, X. Chen, S. M. Wang, and H. Luo, Appl. Phys. Lett. **82**, 4310 (2003).

[74] P. P. Edwards and M. J. Sienko, Phys. Rev. B **17**, 2575 (1978).

[75] C. Timm, J. Phys.: Condens. Matter **15**, R1865 (2003).

[76] A. Efros and B. Shklovskii, *Springer Series in Solid-State Sciences* (Springer, Berlin, 1984).

[77] T. Dietl, F. Matsukura, and H. Ohno, Phys. Rev. B **66**, 033203 (2002).

[78] A. Kaminski and S. Das Sarma, Phys. Rev. Lett. **88**, 247202 (2002).

[79] M. Wang, K. W. Edmonds, B. L. Gallagher, A. W. Rushforth, O. Makarovsky, A. Patanè, R. P. Campion, C. T. Foxon, V. Novak, and T. Jungwirth, Phys. Rev. B **87**, 121301 (2013).

[80] K. W. Edmonds, B. L. Gallagher, M. Wang, A. W. Rushforth, O. Makarovsky, A. Patane, R. P. Campion, C. T. Foxon, V. Novak, and T. Jungwirth, arXiv:1211.3860.

[81] S.-H. Wei, Comput. Mater. Sci. **30**, 337 (2004).

[82] A. Zunger, Appl. Phys. Lett. **83**, 57 (2003).

[83] R. Bouzerar and G. Bouzerar, Europhys. Lett. **92**, 47006 (2010).

[84] H. Peng, J. Li, and S.-H. Wei, Appl. Phys. Lett. **102**, 122409 (2013).

[85] S. Kuroda, N. Nishizawa, K. Takita, M. Mitome, Y. Bando, K. Osuch, and T. Dietl, Nat. Mater. **6**, 440 (2007).

[86] G. Bouzerar, T. Ziman, and J. Kudrnovský, Appl. Phys. Lett. **85**, 4941 (2004).

[87] A. Chakraborty, R. Bouzerar, S. Kettemann, and G. Bouzerar, Phys. Rev. B **85**, 014201 (2012).

[88] Z. Deng, C. Jin, Q. Liu, X. Wang, J. Zhu, S. Feng, L. Chen, R. Yu, C. Arguello, T. Goko *et al.*, Nat. Commun. **2**, 422 (2011).

[89] K. Zhao, B. Chen, G. Zhao, Z. Yuan, Q. Liu, Z. Deng, J. Zhu, and C. Jin, Chin. Sci. Bull. **59**, 2524 (2014).

[90] J. Schneider, U. Kaufmann, W. Wilkening, M. Baeumler, and F. Köhl, Phys. Rev. Lett. **59**, 240 (1987).

[91] M. Pawlowski, M. Piersa, A. Wolos, M. Palczewska, G. Strzelecka, A. Hruban, J. Gosk, M. Kaminska, and A. Twardowski, Acta Phys. Pol. A **108**, 825 (2006).

[92] B. K. Meyer, J. M. Spaeth, and M. Scheffler, Phys. Rev. Lett. **52**, 851 (1984).